Regulatory mechanisms of tau protein fibrillation under the conditions of liquid–liquid phase separation

Solomiia Boyko[a], Krystyna Surewicz[a], and Witold K. Surewicz[a,1]

[a]Department of Physiology and Biophysics, Case Western Reserve University, Cleveland, OH 44106

Edited by Susan Marqusee, University of California, Berkeley, CA, and approved October 27, 2020 (received for review June 16, 2020)

One of the hallmarks of Alzheimer's disease and several other neurodegenerative disorders is the aggregation of tau protein into fibrillar structures. Building on recent reports that tau readily undergoes liquid–liquid phase separation (LLPS), here we explored the relationship between disease-related mutations, LLPS, and tau fibrillation. Our data demonstrate that, in contrast to previous suggestions, pathogenic mutations within the pseudorepeat region do not affect tau441's propensity to form liquid droplets. LLPS does, however, greatly accelerate formation of fibrillar aggregates, and this effect is especially dramatic for tau441 variants with disease-related mutations. Most important, this study also reveals a previously unrecognized mechanism by which LLPS can regulate the rate of fibrillation in mixtures containing tau isoforms with different aggregation propensities. This regulation results from unique properties of proteins under LLPS conditions, where total concentration of all tau variants in the condensed phase is constant. Therefore, the presence of increasing proportions of the slowly aggregating tau isoform gradually lowers the concentration of the isoform with high aggregation propensity, reducing the rate of its fibrillation. This regulatory mechanism may be of direct relevance to phenotypic variability of tauopathies, as the ratios of fast and slowly aggregating tau isoforms in brain varies substantially in different diseases.

tau protein | liquid–liquid phase separation | amyloid | protein aggregation | neurodegenerative diseases

Tau is a major neuronal protein that plays a key role in Alzheimer's disease (AD) and a number of other neurodegenerative disorders that are collectively classified as tauopathies. The latter include frontotemporal dementia with parkinsonism linked to chromosome 17 (FTDP-17), progressive supranuclear palsy, Pick's disease, corticobasal degeneration, and chronic traumatic encephalopathy (1–5). Under normal physiological conditions, tau is localized to axons where it is involved in the assembly of microtubules (1–6). In tauopathies, the protein self-associates into different forms of filaments that contain largely hyperphosphorylated tau and have properties of amyloid fibrils (1–5).

Alternative splicing of the *MAPT* gene that encodes tau results in six major isoforms in the human central nervous system. These isoforms differ with respect to the number of N-terminal inserts as well as the number of 31 to 32 residue pseudorepeat sequences in the C-terminal part of the protein (1–5). Structurally, tau is largely an intrinsically disordered protein, with local secondary structures existing only within the pseudorepeat region (1, 7). A large number of mutations have been identified in the latter region that correlate with inherited cases of FTDP-17 (8, 9). These mutations not only diminish the ability of tau to promote microtubule assembly, but many also promote self-association of tau into amyloid fibrils (10–12). This strongly suggests that tau misfolding and aggregation is one of the key events in disease pathogenesis.

A number of recent reports indicate that purified full-length tau (tau441) has a high propensity to undergo liquid–liquid phase separation (LLPS) in vitro in the presence of crowding agents that emulate the high concentration of macromolecules in the cell. This was observed both for the phosphorylated (13) and nonphosphorylated protein (14–16), and it was determined that tau LLPS is driven largely by attractive electrostatic intermolecular interactions between the negatively charged N-terminal and positively charged middle/C-terminal regions of the protein (15). Tau condensation into droplets (complex coacervation) was also observed in the presence of polyanions such as RNA or heparin (17, 18). These observations in vitro are partially supported by studies in cells (13, 19–24), especially within the context of tau interaction with microtubules (21). However, it remains unclear whether tau could undergo LLPS in cells on its own or, rather, its recruitment to membraneless organelles such as stress granules is largely driven by interactions with other proteins and/or RNA. These limitations notwithstanding, the observations that tau has a propensity for LLPS have potentially important implications for the pathogenic process in tauopathies, as studies with other proteins involved in neurodegenerative diseases (e.g., TDP-43, FUS) indicate that the environment of liquid droplets is conducive to the pathological aggregation of these proteins (25–32). In line with these findings, it was recently suggested that LLPS can initiate tau aggregation. However, the evidence for this was very limited and largely based on optical microscopy observations (13).

In the present study, we explored the relationship between pathogenic mutations of tau, protein LLPS, and aggregation into amyloid fibrils. Our data show that, in contrast to previous suggestions (13), pathogenic mutations within the pseudorepeat region do not affect the propensity of tau to undergo LLPS. These mutations, however, do dramatically accelerate the liquid-to-solid phase transition within the droplets, leading to rapid formation of fibrillar aggregates. Most important, this study also reveals a previously unrecognized mechanism by which

Significance

One of the major pathogenic events in Alzheimer's disease and several other neurodegenerative disorders is the aggregation of tau protein into fibrillar structures. Recent reports demonstrated that tau can undergo liquid–liquid phase separation, forming liquid droplets. The key finding of the present study is that liquid–liquid phase separation uniquely regulates the rate of tau fibrillation in mixtures containing tau isoforms with different aggregation propensities. Given that, due to alternative splicing, the proportions of fast and slowly aggregating tau isoforms in brain vary substantially in different tauopathies, this previously unrecognized regulatory mechanism may play an important role as one of the major determinants of phenotypic variability within this class of neurodegenerative diseases.

Author contributions: S.B. and W.K.S. designed research; S.B. and K.S. performed research; S.B. and W.K.S. analyzed data; and S.B. and W.K.S. wrote the paper.

The authors declare no competing interest.

This article is a PNAS Direct Submission.

[1]To whom correspondence may be addressed. Email: wks3@case.edu.

This article contains supporting information online at https://www.pnas.org/lookup/suppl/doi:10.1073/pnas.2012460117/-/DCSupplemental.

First published December 1, 2020.

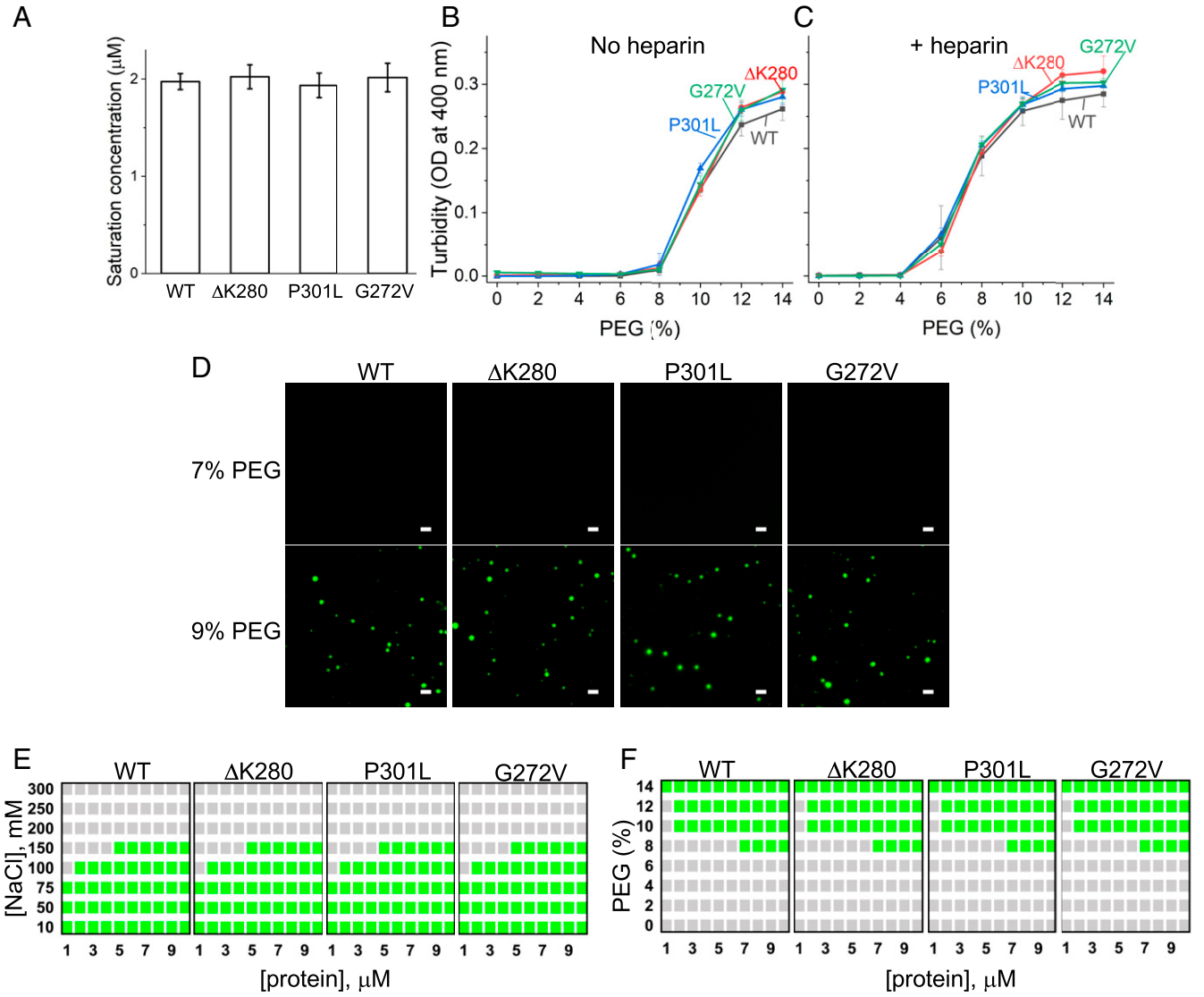

Fig. 1. Disease-related mutations (ΔK280, P301L, and G272V) have no effect on LLPS of tau441 protein. (*A*) Saturation concentrations for wild-type tau 441 and tau441 variants with disease-related mutations in the presence of 10% PEG-10. Error bars represent SD ($n = 4$). (*B* and *C*) LLPS of wild-type tau441 and disease-related tau441 mutants (5 μM each) in the absence (*B*) and presence (*C*) of heparin monitored by turbidity (OD at 400 nm) as a function of PEG-10 concentration. The molar ratio of heparin to protein in heparin-containing samples was 2:1. Error bars represent SD ($n = 3$). (*D*) Representative fluorescence microscopy images of wild-type tau441 and disease-related tau441 mutants (5 μM in each case) in the presence of 7% (*Top*) and 9% (*Bottom*) PEG-10. The images were obtained using 1:10 mixtures of Alexa Fluor 488-labeled and unlabeled proteins. (Scale bar, 3 μm.) (*E* and *F*) Phase diagrams for wild-type and mutant tau441. (*E*) Protein concentration versus NaCl concentration phase diagram. (*F*) Protein concentration versus PEG-10 concentration phase diagram. Gray and green boxes indicate the absence and presence of phase separation, respectively. All experiments were performed in 10 mM Hepes buffer (pH 7.4) containing 100 mM NaCl, 1 mM DTT, and 2 mM EDTA.

LLPS can regulate the rate of amyloid formation in mixtures containing tau isoforms with different aggregation propensities. These findings strongly suggest that LLPS may play a major regulatory role in the formation of pathological tau aggregates in neurodegenerative diseases.

Results

The Effect of Pathogenic Mutations on Tau LLPS. Many of the mutations associated with familial cases of FTDP-17 have a profound effect on physicochemical properties of tau (8–12). Therefore, we first asked the question whether these mutations could also affect the propensity of tau to undergo LLPS. To probe this issue, we focused on three selected mutations within the pseudorepeat region, G272V, P301L, and ΔK280. These mutations, which are among the most extensively studied, have been reported to increase the aggregation propensity of tau in the absence of LLPS (10–12).

To assess the effect of these mutations on tau441 propensity for LLPS, we determined saturation concentrations of all tau441 variants studied, a commonly used measure of protein capacity to undergo LLPS (33). This was done by measuring the turbidity (in the presence of a crowding agent, 10% polyethylene glycol with a molecular weight of 10 kDa [PEG-10]) as a function of protein concentration (*SI Appendix*, Fig. S1*A*). As shown in Fig. 1*A*, saturation concentrations of all four proteins were essentially identical, indicating that none of the mutations tested affects the ability of tau441 to undergo LLPS. To further verify this conclusion, we assessed the extent of LLPS at one selected protein concentration (5 μM) in the presence of increasing concentrations of PEG-10. Turbidity versus PEG-10 concentration

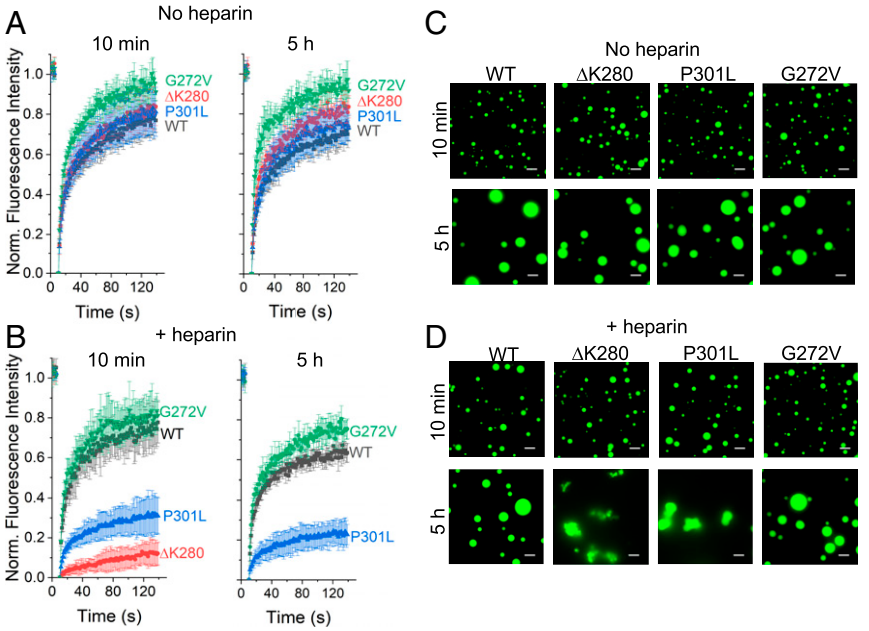

Fig. 2. The effect of disease-related mutations on the maturation of tau441 droplets. (*A* and *B*) Representative FRAP traces for droplets prepared from wild-type tau441 and disease-related tau441 mutants (20 μM in each case) in the absence (*A*) or presence (*B*) of heparin (40 μM). The images were obtained 10 min (*Left*) or 5 h (*Right*) after LLPS induction by addition of 10% PEG-10. Each trace represents an average of measurements for at least six droplets; error bars represent SD. (*C* and *D*) Representative fluorescence microscopy images of wild-type tau441 and disease-related tau441 mutants (20 μM protein, 1:10 ratio of Alexa Fluor 488-labeled to unlabeled protein) in the absence (*C*) or presence (*D*) of heparin (40 μM). The images were obtained 10 min (*Top*) or 5 h (*Bottom*) after LLPS induction by addition of 10% PEG-10. (Scale bar, 10 μm.) All experiments were performed in 10 mM Hepes buffer (pH 7.4) containing 100 mM NaCl, 1 mM DTT, and 2 mM EDTA.

plots for all three tau441 mutants studied were very similar to that for the wild-type protein (Fig. 1*B*). Consistent with these data, no droplets were detected by fluorescence microscopy for any of the protein variants (5 μM in each case) at 7% PEG-10 (i.e., just below the threshold PEG-10 concentration at which a sharp turbidity increase was observed), but for all of them droplets could be seen in the presence of 9% PEG-10 (i.e., just above the threshold PEG-10 concentration) (Fig. 1*D*). To assess the relative LLPS propensity of different tau mutants under a broader range of conditions, we constructed protein concentration versus NaCl concentration and protein concentration versus PEG-10 concentration phase diagrams (Fig. 1 *E* and *F*). These phase diagrams were essentially identical for wild-type and mutant proteins, indicating that the interactions driving phase separation of tau are not altered in the presence of pathogenic mutations tested. To further verify this conclusion, we tested the effect of 1,6-hexanediol, a compound known to inhibit LLPS of some proteins, presumably by disrupting hydrophobic interactions. The 1,6-hexanediol had no effect on LLPS of any of tau variants tested (*SI Appendix*, Fig. S1*B*).

Polyanions such as heparin or RNA are required as cofactors for tau fibrillation in vitro (1, 3, 5). These polyanions have also been shown to form electrostatically driven complex coacervates with the protein, even though only under the conditions of very low ionic strength (17, 18). Therefore, we continued our study probing the ability of pathogenic mutations to affect tau LLPS in the presence of one of such fibrillation-promoting polyaninic cofactors, low molecular weight heparin. For all protein variants (5 μM in each case), heparin (used at the 2:1 molar ratio of heparin to protein) decreased the threshold PEG-10 concentration required to induce LLPS from ∼9% in the absence of any polyanion to ∼4% (Fig. 1 *B* and *C*). However, akin to the observation in the absence of heparin, the turbidity versus PEG-10 concentration plots for all three tau441 variants studied were essentially identical and indistinguishable from that for the wild-type protein. Altogether, the present data in the absence and presence of heparin clearly demonstrate that, contrary to previous suggestions (13), disease-related point mutations in the pseudorepeat region do not affect the propensity of tau to undergo LLPS in any significant manner.

Tau Pathogenic Mutations Alter Material Properties of Liquid Droplets. To explore the effect of these mutations on the material properties of tau droplets, we performed fluorescence recovery after photobleaching (FRAP) experiments. In the absence of heparin, freshly formed droplets for all tau441 variants studied exhibited rapid fluorescence recovery (at least ∼80% within 120 s, with the highest recovery consistently observed for the G272V variant), indicating the highly dynamic nature of proteins within the droplet phase (Fig. 2 *A*, *Left*). Upon incubation at 37 °C for 5 h, droplets formed by all tau441 variants grew in size (Fig. 2*C*). Remarkably, however, all incubated droplets still retained a highly dynamic character, as indicated by only slightly reduced maximum fluorescence recovery after photobleaching than that observed for fresh droplets (Fig. 2*A*). Thus, in the absence of any polyanionic cofactors, droplets formed by both the wild-type and mutant tau441 appear to remain highly dynamic even for many hours after formation, with little tendency of the proteins within droplets' interior to assemble into solid-like aggregates.

The picture looked quite different when droplets were generated in the presence of heparin. In this case, FRAP experiments indicated that wild-type and G272V tau441 droplets were still liquid-like and dynamic even 5 h after formation (Fig. 2*B*, *Right*). In sharp contrast, droplets formed by the ΔK280 tau441 variant exhibited essentially no recovery of fluorescence signal after photobleaching already within 10 min after formation (Fig. 2*B*). Even though at this early stage ΔK280 tau441 droplets were still spherical (Fig. 2*D*, *Top*), fluorescence microscopy images recorded upon "aging" revealed the presence of particles of

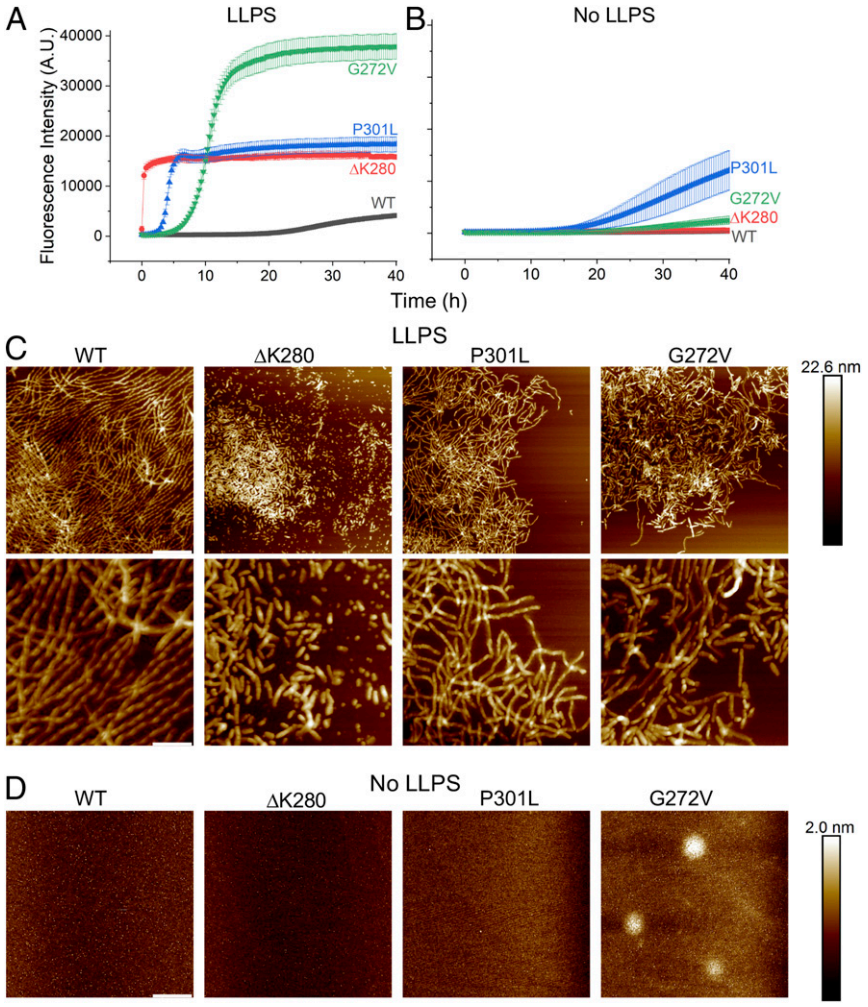

Fig. 3. Mutation-dependent accelerating effect of LLPS on fibrillation of tau441. (*A*) ThT fluorescence traces for wild-type tau441 and disease-related tau441 mutants (5 μM protein, 10 μM heparin in each case) under the conditions of LLPS (*A*) or in the absence of LLPS (*B*). A.U., arbitrary units. Error bars represent SD ($n = 6$ to 9). (*C*) Representative atomic force microscopy images for wild-type tau441 and disease-related tau441 mutants obtained at the end of the growth phase of fibrillation reaction for each protein under LLPS conditions (30, 2, 9, and 22 h for the wild-type tau441and the ΔK280, P301L, and G272V variants, respectively). (Scale bars, 660 nm [*Top*] and 220 nm [*Bottom*].) (*D*) Representative atomic force microscopy images for individual proteins in the absence of LLPS at the same time points as in *C*. (Scale bar, 660 nm.) Fibrillation reactions were carried out in 10 mM Hepes buffer (pH 7.4) containing 100 mM NaCl, 1 mM TCEP, and 2 mM EDTA. LLPS was induced by the addition of 10% PEG-10.

irregular and variable shape (Fig. 2*D*, *Bottom*), suggesting protein aggregation. This is in contrast to the wild-type and G272V tau441 droplets that remained spherical and highly dynamic even after 5 h incubation (Fig. 2 *D*, *Bottom*). P301L tau441 droplets showed an intermediate behavior; they were losing dynamicity with time, but not as fast as ΔK280 tau441 droplets. Upon aging, these droplets remained spherical, clumping together with apparently reduced ability to fuse into larger droplets (Fig. 2*D*). Thus, it appears that aging-dependent material properties of tau441 droplets formed in the presence of heparin are modulated by pathogenic mutations, with ΔK280 mutation resulting in a rapid liquid-like to solid-like transition of the protein within the droplet interior and P301L mutation having a more modest solidification effect.

To further verify this conclusion, we employed a salt resistance assay which takes advantage of a very strong sensitivity of freshly prepared droplets to treatment with high concentrations of NaCl, and gradual loss of this sensitivity when droplets become more rigid with time (34). This assay clearly confirmed FRAP data, further demonstrating rapid loss of dynamicity of droplets formed by ΔK280 tau441, slower solidification of P301L tau441 droplets, and very slow (if any) solidification of wild-type and G272V tau441 droplets (*SI Appendix*, Fig. S2).

Mutation-Dependent Acceleration of Tau Fibrillation under LLPS Conditions. Next, we sought to determine how the environment of liquid droplets affects the ability of tau441 and its pathogenic mutants to aggregate into amyloid fibrils. To this end, we monitored fibril formation of tau441 variants (5 μM each) in the presence of 10 μM heparin and 10% PEG-10 using a thioflavin T (ThT) fluorescence assay. Under these conditions, the amount of protein outside the droplets was very low, as indicated by the saturation concentration of ∼0.4 μM (*SI Appendix*, Fig. S3). This allows an unambiguous interpretation of experimental data, since at such low concentration, fibrillation of tau441 is very slow and the protein outside droplets should have no significant contribution to the ThT fluorescence signal.

The ThT fluorescence curves shown in Fig. 3 demonstrate that, for all tau441 variants studied, LLPS results in a dramatic acceleration of the fibrillation reaction. For the wild-type protein, the lag phase of the reaction under LLPS conditions was ∼16 h (Fig. 3*A*). In sharp contrast, no measurable increase in

ThT fluorescence intensity was observed up to at least 40 h for the reaction in the absence of LLPS (Fig. 3*B*). This effect was even stronger for the mutant proteins (Fig. 3 *A* and *B*). For example, for the P301L variant, the lag phase was reduced from ∼17 h in the absence of LLPS (Fig. 3*B*) to ∼3 h in the droplet environment (Fig. 3*A*), and the rate of the growth phase was also greatly increased. The rate of fibrillation under LLPS conditions was especially high for the ΔK280 variant. In the latter case, the reaction (without any measurable lag phase) was essentially completed within 30 min (Fig. 3*A*), in sharp contrast to the lack of any ThT fluorescence increase up to at least 40 h in the absence of LLPS (Fig. 3*B*). The final ThT intensities at the end of the growth phase under LLPS conditions were different for individual tau variants (Fig. 3*A*). Even though the molecular basis of this finding remains at present unclear, different amplitudes of ThT signal may reflect mutation-dependent structural differences of tau fibrils and/or differences in fibril packing densities within the droplets.

The morphology of aggregates formed under LLPS conditions was examined by atomic force microscopy (AFM). The images (at two different magnifications) obtained at the end of the growth phase for each protein are shown in Fig. 3*C*. Both for the wild-type protein as well as the pathogenic variants, discrete regions of densely packed networks of fibrillar structures and the regions lacking these structures were observed on the mica surface, consistent with the notion that fibrils were formed within the droplets. While for the wild-type tau441 these fibrils appeared as twisted, helical structures similar to those reported for tau fibrils in the absence of LLPS (1, 3, 35), fibrils formed by the ΔK280 tau441 variant had clearly distinct morphology, appearing as short, straight rods. Morphological differences between wild-type tau441 and the P301L or G272V variants were more difficult to ascertain by AFM, especially since individual fibrils could be seen only at the edges of the densely packed clumps. Importantly, consistent with the ThT data, no fibrillar structures were observed in AFM images for individual proteins at the same time points under the conditions of no LLPS (Fig. 3*D*).

A dramatic acceleration of tau fibrillation under LLPS conditions as described above was observed when droplets were formed from the mixture of tau441 variants and heparin. However, tau in a crowded environment (that mimics physiologically relevant conditions) can also form liquid droplets in the absence of heparin or other polyanions. Thus, the questions arise whether the latter droplets could recruit polyanions from the external environment, and whether this recruitment of the cofactor to preexisting droplets could initiate rapid fibrillation of the protein. To address these questions, we formed (in the presence of 10% PEG-10, but in the absence of heparin) droplets from Alexa Fluor 488-labeled tau441 variants alone and, after 1-h incubation, added to the suspension of these droplets rhodamine-labeled heparin. Representative fluorescence microscopy images for ΔK280 tau441 clearly demonstrated that heparin was immediately incorporated into the droplets (*SI Appendix*, Fig. S4 *A* and *B*). Importantly, this recruitment of heparin into preexisting tau droplets resulted in a rapid loss of droplet dynamicity, as indicated by FRAP experiments (*SI Appendix*, Fig. S4*C*). This was followed by a rapid, lag phase-free fibrillation reaction, as indicated by ThT fluorescence measurements (*SI Appendix*, Fig. S4*D*). A similar phenomenon was observed for other tau441 variants studied, as exemplified by fast fibrillation reactions upon heparin addition to protein droplets (*SI Appendix*, Fig. S4*E*). Thus, the recruitment of polyanionic cofactors such as heparin from the bulk phase into preexisting tau droplets can lead to greatly accelerated aggregation of the protein into amyloid fibrils.

Regulation of Tau Fibrillation Kinetics under LLPS Conditions. The overall rate of the fibrillation reaction in the absence of LLPS should increase with increasing protein concentration (36, 37). Such a dependence could indeed be observed for all tau441 variants, as exemplified in Fig. 4*A* for P301L tau441. However, under LLPS conditions (i.e., in the two-phase regime) tau441 concentration in the dilute and condensed phases under given experimental conditions should be constant; only the relative volume fractions of the two phases would change as a function of total protein concentration in the system (33). Thus, in this case, the fibrillation rate should not change when total protein concentration is increased. To test this prediction, we measured the kinetics of P301L tau441 fibrillation in the presence of 10% PEG-10, finding that both the lag times as well as the growth rates were indeed essentially identical when experiments were performed using different protein concentrations (Fig. 4*B*). The only difference was observed with regard to the final intensity of ThT fluorescence. The latter was proportional to protein concentration, indicating that the volume occupied by the condensed phase (and thus the amount of protein in this phase) scale with total protein concentration in the system. A similar phenomenon was observed for all other tau441 variants studied (*SI Appendix*, Fig. S5).

Based on these observations, we explored the potential mechanisms by which protein aggregation could be regulated in the context of LLPS. We hypothesized that this could be accomplished by the recruitment of other proteins that "dilute" the aggregation-prone species within droplets. To test this hypothesis, we performed experiments in which droplets were formed (in the presence of 10% PEG-10 and heparin) from mixtures of fibrillation-prone tau441 variants (i.e., either wild-type tau441 or any of its pathogenic mutants tested) and ΔPHF6*ΔPHF6 tau441 in which residues 275 to 280 and 306 to 311 were deleted. While these deletions greatly compromise the ability for tau to undergo fibrillation (38, 39), they have a marginal effect on protein capacity to undergo LLPS (*SI Appendix*, Fig. S6).The mixtures of ΔPHF6*ΔPHF6 tau441 and any of the fibrillation-competent tau variants studied appear to be fully miscible within the droplets, forming a single condensed phase as indicated by fluorescence microscopy (Fig. 5*A*). Remarkably, under LLPS conditions, the addition of an equimolar proportion of ΔPHF6*ΔPHF6 tau441 to wild-type tau441 (5 μM each) resulted in a strong decrease of the fibrillation rate of the latter protein, with the lag time increasing from ∼16 to ∼30 h (Fig. 5*B*). This effect was even more dramatic when the proportion of ΔPHF6*ΔPHF6 tau441 was increased, with no fibrillation observed up to at least 55 h at a tau441 to ΔPHF6*ΔPHF6 tau441

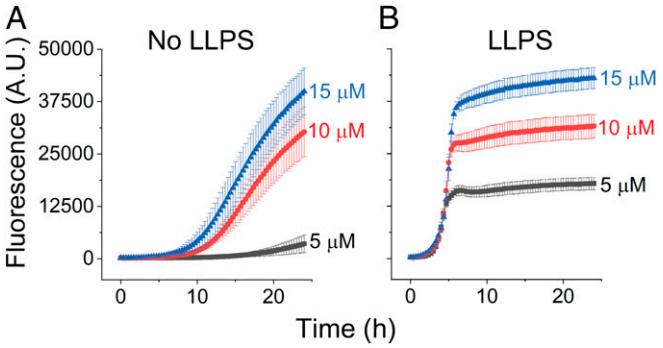

Fig. 4. Kinetics of P301L tau441 fibrillation at different protein concentrations in the absence of LLPS (*A*) and under the conditions of LLPS (*B*). The fibrillation reactions were monitored by ThT fluorescence in the presence of heparin (1:2 molar ratio of protein to heparin) in 10 mM Hepes buffer (pH 7.4) containing 100 mM NaCl, 1 mM TCEP, and 2 mM EDTA. LLPS was induced by the addition of 10% PEG-10. The numbers at individual traces indicate total protein concentration in the system. Error bars represent SD ($n > 6$). A.U., arbitrary units.

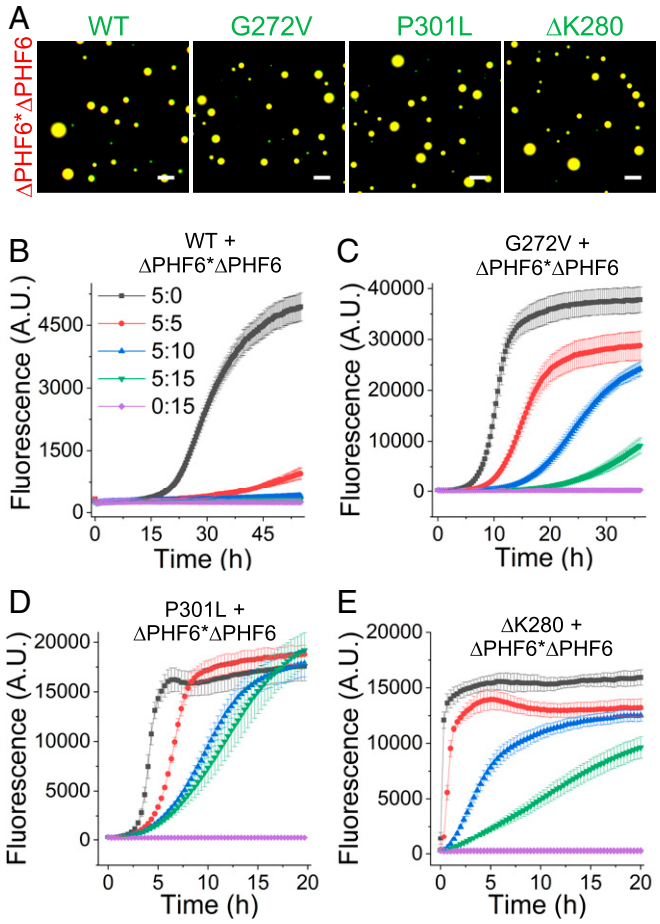

Fig. 5. Corecruitment of ΔPHF6*ΔPHF6 tau441 into liquid droplets decreases fibrillation rate of the aggregation-prone tau species. (*A*) Representative fluorescence microscopy images demonstrating colocalization and miscibility of ΔPHF6*ΔPHF6 tau441 and all aggregation-prone tau variants studied within liquid droplets. The mixture of ΔPHF6*ΔPHF6 tau441 with wild-type tau441 or the disease-related mutants (5 μM each) contained 10% of Alexa Fluor 594-labeled ΔPHF6*ΔPHF6 tau441 (red) and Alexa Fluor 488-labeled (green) respective partner proteins. Colocalization within droplets results in yellow fluorescence. (Scale bars, 5 μm.) (*B–E*) ThT fluorescence traces for fibrillation reactions of wild-type tau441 and disease-related tau mutants (5 μM in each case) in the presence of increasing concentration of ΔPHF6*ΔPHF6 tau441 (5, 10, and 15 μM) under LLPS conditions in the presence of heparin (total protein to heparin molar ratio of 1:2). The numbers in a color-coding scheme shown in *B* (that applies also to all other panels) indicate concentrations (in micromoles) of the aggregation-prone tau variant (first number) and ΔPHF6*ΔPHF6 tau441 (second number). Error bars represent SD (n = 5 to 9). Experiments were performed in 10 mM Hepes buffer (pH 7.4) containing 100 mM NaCl, 1 mM TCEP, 2 mM EDTA, and 10% PEG-10.

molar ratio of 2:1. This "dilution effect" under LLPS conditions was also observed for the mixtures of ΔPHF6*ΔPHF6 tau441 with all three pathogenic tau mutants studied: corecruitment of ΔPHF6*ΔPHF6 tau441 to the droplets of each of these pathogenic proteins resulted in a much slower fibrillation rate, and this effect became increasingly dramatic when the proportion of ΔPHF6*ΔPHF6 tau was increased (Fig. 5 *C–E*). A similar phenomenon was observed in mixtures of wild-type tau441 or its pathogenic mutants with other nonaggregating tau variants, I277P/I308P 2N4R tau and I308P 2N3R tau (39), as exemplified for wild-type and P301L tau441 (*SI Appendix*, Fig. S7).

Building on this intriguing finding, we next asked whether a similar regulatory mechanism could also be operational in the case of more physiologically relevant mixtures of full-length tau441 variants (that contain all four pseudorepeats, i.e., 2N4R isoforms) with the 2N3R tau isoform (in which the second pseudorepeat is missing). To explore this issue, first we examined the mixture of P301L tau441 (i.e., P301L 2N4R tau) and 2N3R tau (that lacks the region containing the mutation site). This system provides an especially useful model, as spontaneous fibrillation of 2N3R under LLPS conditions is much slower than that of P301L 2N4R tau (40) (Fig. 6*B*), and recent data indicate that P301L 2N4R tau fibrils cannot seed 2N3R tau (41). Akin to the observation for the mixtures containing ΔPHF6*ΔPHF6 tau441, corecruitment of 2N3R tau to liquid droplets greatly reduced the rate of P301L 2N4R tau fibrillation (Fig. 6*B*), and this effect appeared to be even somewhat more pronounced compared to that found for ΔPHF6*ΔPHF6 tau441 or I277P/I308P tau441 (Fig. 5*D* and *SI Appendix*, Fig. S7*B*). A similar

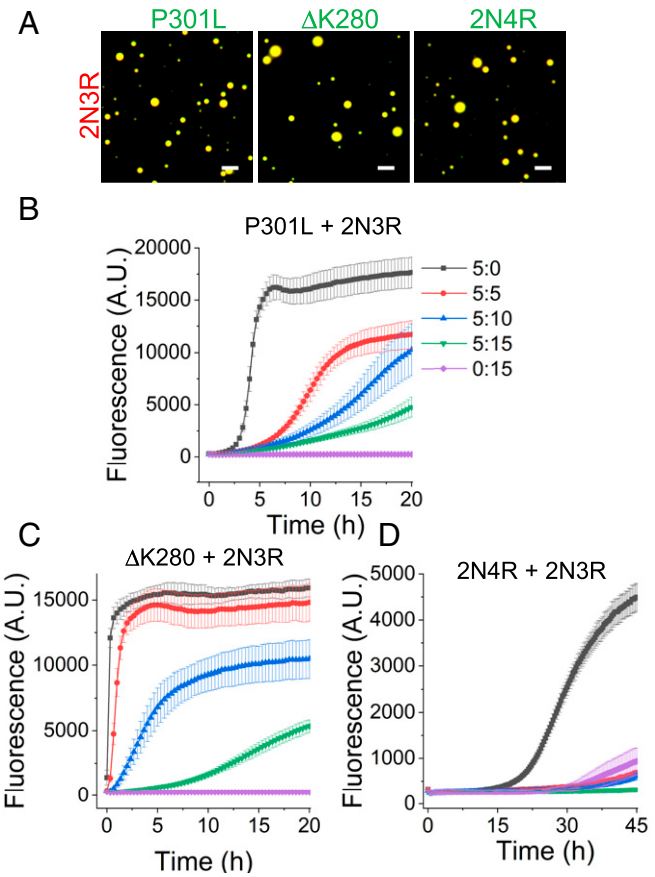

Fig. 6. Corecruitment of 2N3R tau into liquid droplets decreases fibrillation rate of wild-type tau441 (i.e., the 2N4R isoform) and disease-related 2N4R tau mutants. (*A*) Representative fluorescence microscopy images demonstrating colocalization and miscibility of 2N3R tau with P301L, ΔK280, and wild-type 2N4R within liquid droplets. The mixture of 2N3R with wild-type tau441 or the disease-related mutants (5 μM each) contained 10% of Alexa Fluor 594-labeled 2N3R tau (red) and Alexa Fluor 488-labeled (green) respective partner proteins. Colocalization within droplets results in yellow fluorescence. (Scale bars, 5 μm.) (*B–D*) ThT fluorescence traces for 2N4R tau and disease-related 2N4R tau mutants (5 μM in each case) in the presence of increasing concentration of 2N3R tau (5, 10, and 15 μM) under LLPS conditions in the presence of heparin (total protein to heparin molar ratio of 1:2). The numbers in a color-coding scheme shown in *A* (that applies also to other panels) indicate concentrations (in micromoles) of the 2N4R tau isoform (first number) and the 2N3R isoform (second number). Error bars represent SD (n = 5 to 11). Experiments were performed in 10 mM Hepes buffer (pH 7.4) containing 100 mM NaCl, 1 mM TCEP, 2 mM EDTA, and 10% PEG-10.

decrease in fibrillation kinetics upon the addition of 2N3R tau was observed for ΔK280 2N4R tau (Fig. 6*C*), another pathogenic variant that forms fibrils which, under LLPS conditions, cannot seed fibrillation of 2N3R tau, as determined in the present study (*SI Appendix*, Fig. S8*A*). Finally and most remarkably, a large decrease in the fibrillation rate in the presence of 2N3R tau was also observed for wild-type 2N4R tau (Fig. 6*D*), despite the ability of fibrils formed by the latter protein to seed fibrillation of 2N3R tau (*SI Appendix*, Fig. S8*A*). This underscores a far-reaching impact of the dilution effect due to corecruitment of two proteins into the condensed phase. In the case of the wild-type 2N4R/2N3R tau mixture, this dilution greatly reduces the rate of spontaneous fibrillation of the normally fast aggregating 2N4R isoform and, as a consequence of it, also delays 2N4R tau amyloid-seeded fibrillation of a more slowly aggregating 2N3R tau.

Discussion

Numerous lines of evidence point to a strong link between LLPS of certain proteins and the pathogenic process in neurodegenerative diseases (27–32), even though molecular level details of this link are still poorly understood. One of the key arguments in support of a direct mechanistic connection between LLPS and disease pathogenesis is that disease-causing mutations in proteins such as TDP43 (42), FUS (25), hnRNPA1 (43), hnRNPAA (44), or TIA1 (45) lead to disturbances in membraneless organelles in cells and/or liquid droplets formed in vitro. The mechanisms of these disturbances appear, however, to be protein and even mutation specific, with some mutations promoting LLPS (e.g., TIA1 mutations) (45) and others having an opposite effect (e.g., most mutations in TDP43) (42). Furthermore, the consequences of LLPS with regard to protein aggregation may also be protein specific (31).

Based on limited optical microscopy data, it was recently postulated that pathogenic mutations in tau441 (including, among others, P301L and ΔK280 mutations) promote formation of liquid droplets (13, 16), and that this enhanced LLPS capacity is related to increased β-sheet propensity of these mutant proteins (13). However, our present data do not support this scenario, clearly demonstrating that, under the conditions used in the present experiments, none of the three mutations tested (P301L, ΔK280, and G272V) affects in any measurable way the propensity of tau441 to form liquid droplets. This present finding is consistent with our recently proposed mechanistic model of tau441 LLPS, according to which phase separation is driven by intermolecular attractive interactions between the negatively charged N-terminal and positively charged middle/C-terminal regions of the protein (15). Since these electrostatic interactions are a global property of the entire molecule and involve a great many residues, removal of just one positive charge in the ΔK280 variant should not affect the capacity for LLPS. An unaltered propensity of the P301L and G272V variants to form liquid droplets is even easier to rationalize, as none of these mutations involve charged residues. This apparent insensitivity of tau441 capacity for LLPS to disease-related mutations is different from the situation observed for proteins such as TDP43. In the latter case, LLPS is mediated by well-defined intermolecular contacts involving specific amino acid residues, and disease-related mutations that interfere with these contacts significantly alter phase separation properties of the protein (42).

Despite the apparent neutrality of pathogenic mutations with regard to tau propensity for LLPS, ΔK280 and P301L mutations induce rapid transition within liquid droplets to less dynamic assemblies, as demonstrated by FRAP measurements. Such an acceleration of droplet "solidification" in the presence of disease-related mutations has been previously observed for several RNA binding proteins involved in amyotrophic lateral sclerosis and frontotemporal dementia (25, 43–45). The present finding that a similar phenomenon occurs upon introduction of pathogenic mutations into tau protein (that is structurally and functionally unrelated to these RNA binding proteins) further supports the hypothesis that a mutation-accelerated transition within liquid droplets to more stable solid-like assembles is of direct relevance to the pathogenic process in neurodegenerative diseases. In the case of tau, this solidification is followed by a second transition to fibrillar aggregates (filaments) that are one of the hallmarks of Alzheimer's diseases and several other disorders. Even though tau441 can form fibrils in the absence of LLPS (1, 3, 10), the present data demonstrate that this reaction is greatly accelerated in the environment of originally liquid-like droplets. Again, this effect becomes particularly strong for tau variants with disease-related mutations, as exemplified by ΔK280 tau441, which undergoes especially rapid fibrillation under LLPS conditions, with no detectable lag phase. The lack of correlation between the intrinsic LLPS propensity of pathogenic tau variants (which is essentially identical for wild-type and mutant proteins) and mutation-dependent acceleration of droplet solidification and fibril formation strongly suggests that different types of interactions drive tau LLPS per se and protein fibrillation within droplets.

The mechanism by which individual tau mutations accelerated fibril formation is not fully understood. In the absence of LLPS, it has been suggested that mutations such as ΔK280 and P301L may produce this effect by inducing conformational changes within the pseudorepeat domain and thereby creating a hydrophobic surface (ΔK280) or extending the aggregation-prone β-strand (P301L) (11). Similar mechanisms may also be operational under the conditions of LLPS, especially given that the relative capacity of individual mutations to increase fibrillation propensity within droplets correlates with that reported in the absence of phase separation (11). A dramatic acceleration of tau441 fibrillation under LLPS conditions is likely in large part due to greatly increased protein concentration in the condensed phase. However, other factors may also contribute to this effect, including a possibility that the environment of liquid droplets alters the conformation of tau protein, making it more open and, therefore, more prone to fibrillation. On the other hand, very high viscosity within droplets would be expected to slow down the fibrillation reaction. Thus, the rate of protein aggregation under the conditions of LLPS is a net result of all these factors.

The most intriguing finding of this study is the unique regulatory mechanisms of tau aggregation under the conditions of LLPS. Our data clearly demonstrate that, when two tau isoforms with different fibrillation propensities are recruited into liquid droplets, the fibrillation rate of the rapidly aggregating species may be greatly decreased by the presence of another tau species with lower aggregation propensity. This is because, under the given conditions, total concentration of all tau variants within the condensed phase is constant; therefore, the slowly aggregating (or nonaggregating) tau variant effectively lowers the concentration of the variant with high aggregation propensity, reducing the rate of its fibrillation. This behavior is fundamentally different from the situation in the absence of LLPS, in which case no such dilution effect could occur, as the addition of lower aggregation propensity tau species to the solution of high aggregation propensity species does not affect the concentration of the latter protein.

This previously unrecognized regulatory mechanism of protein aggregation within liquid droplets may be of direct relevance to the molecular basis of phenotypic variability of tauopathies, as the ratios of 4R (rapidly aggregating species) to 3R (more slowly aggregating species) tau isoforms varies substantially in different diseases. For example, in sporadic cases of Alzheimer's disease this ratio is believed to be around 1:1 (8, 9). By contrast, progressive supranuclear palsy and corticobasal degeneration are considered to be largely 4R tauopathies (8, 9, 46, 47), whereas Pick's disease is largely a 3R tauopathy (48). Furthermore,

specific MAPT mutations associated with familial forms of tauopathies are known to affect splicing in different ways, resulting in different ratios of the 4R and 3R isoforms (8, 9). For example, while ΔK280 and G272V mutations are associated with predominance of the 3R isoform, P301L and N279K mutations lead to increased expression of 4R tau (8, 9). This variability of relative populations of the 4R and 3R isoforms, combined with our present findings regarding the regulatory effect of one tau isoform on fibrillation kinetics of another isoform, suggests that LLPS could provide a powerful mechanism for controlling the rate of tau aggregation in different types of tauopathies. These findings may also have more general implications, as a similar dilution effect could potentially be operational for other LLPS- and aggregation-prone proteins that exist in several isoforms due to alternative splicing.

The present findings were made using bacterially expressed tau which is nonphosphorylated. Thus, the question remains how phosphorylation affects tau LLPS per se and how it impacts the link between LLPS and pathological aggregation. Furthermore, it should be noted that membraneless organelles in which tau was found to colocalize in cells contain many other proteins as well as RNA (20). These additional macromolecules cannot (and likely do not) only facilitate tau recruitment to stress granules but also contribute to regulatory mechanisms of tau aggregation in these organelles. The present findings in a relatively simple model in vitro provide a conceptual foundation for future studies in more complex systems.

Materials and Methods

Expression, Purification, and Labeling of Tau Variants. Tau variants were expressed and purified as described previously (15). Protein concentration was determined using a reducing agent-compatible bicinchoninic acid (BCA) protein assay (Thermo Fisher Scientific). Proteins were fluorescently labeled with Alexa Fluor 488 or Alexa Fluor 594 dye (Invitrogen) as described previously (15).

Turbidity Measurements. LLPS was monitored by turbidity (optical density at 400 nm) at 37 °C using the M1000 Tecan plate reader. Experiments were carried out in 10 mM Hepes buffer (pH 7.4) containing 1 mM dithiothreitol (DTT), 2 mM ethylenediaminetetraacetic acid (EDTA), 100 mM NaCl, and freshly prepared PEG 10,000 (PEG-10) (Sigma-Aldrich).

Fluorescence Microscopy Imaging. Droplets of tau variants were formed in 10 mM Hepes buffer (pH 7.4) containing 1 mM DTT, 2 mM EDTA, 100 mM NaCl, and freshly prepared PEG-10. Droplets were visualized by fluorescence microscopy using Alexa Fluor 488- or Alexa Fluor 594-labeled tau variants that were mixed with unlabeled proteins at a molar ratio of 1:10. To visualize heparin recruitment to liquid droplets, rhodamine-labeled heparin (Creative PEGWorks) was used. Samples (20 μL) were placed on the glass bottom of a 35-mm dish precoated with 1% Pluronic F-127 (Sigma). Microscopy experiments were performed at room temperature on a Keyence BZ-X710 microscope with a ×100/1.45 numerical aperture oil-immersion lens.

FRAP. Samples for FRAP were prepared as described above for fluorescence microscopy imaging experiments. FRAP measurements were performed using a Leica HyVolution SP8 confocal microscope with 2.4-mW laser intensity for bleaching, ×63/1.4 numerical aperture oil-immersion objective, and photomultiplier tube detector. Regions of interest (0.35-μm diameter) were bleached within ∼5-μm droplets. The measurements involved five prebleaching frames, three flashes of bleaching (16.8% of laser power), and 100 postbleaching frames (1.3 s/frame). Individual FRAP traces were normalized to maximal prebleach and minimal postbleach intensities.

Thioflavin T Fluorescence Assay. The fibrillization reactions were carried out in 10 mM Hepes buffer (pH 7.4) containing 1 mM Tris(2-carboxyethyl)phosphine (TCEP), 2 mM EDTA, 100 mM NaCl, 0.02% sodium azide, 20 μM ThT, and low molecular weight heparin (4.4 kDa, Celsus Laboratories). The molar ratio of protein to heparin in all experiments was 1:2. LLPS was induced by the addition of 10% freshly prepared PEG-10. Fluorescence was monitored on the M1000 Tecan plate reader (excitation and emission wavelengths of 440 and 485 nm, respectively). Experiments were performed at 37 °C under quiescent conditions, with measurements taken every 20 min. In the seeded reactions, a small amount (5%) of fibrils preformed under LLPS conditions was added to tau monomers. Before use, the seeds were subjected to sonication in order to break down larger clumps.

Atomic Force Microscopy Imaging. Atomic force microscopy imaging was performed as described previously (26). Samples were deposited on freshly cleaved mica substrate, left at room temperature for 3 min, then washed three times with Milli-Q water and dried under N_2. The images were obtained using scan assist mode and a silicon probe (spring constant, 40 N/m) on a Bruker multimode atomic force microscope equipped with a Nanoscope V controller. Image processing was performed using the Nanoscope Analysis software.

Data Availability. All study data are included in the article and supporting information.

ACKNOWLEDGMENTS. We thank Michael Babinchak, Virender Singh, and Ling Xu for critical comments on this manuscript. This work was supported by NIH grant RF1 AG061797 (W.K.S.) and the Pilot Project Grant from the Department of Physiology and Biophysics, Case Western Reserve University. The microscopy facility was supported by NIH Office of Research Infrastructure Programs grant S10 OD024996.

1. E. M. Mandelkow, E. Mandelkow, Biochemistry and cell biology of tau protein in neurofibrillary degeneration. *Cold Spring Harb. Perspect. Med.* **2**, a006247 (2012).
2. K. Iqbal, F. Liu, C. X. Gong, Tau and neurodegenerative disease: The story so far. *Nat. Rev. Neurol.* **12**, 15–27 (2016).
3. M. Goedert, D. S. Eisenberg, R. A. Crowther, Propagation of tau aggregates and neurodegeneration. *Annu. Rev. Neurosci.* **40**, 189–210 (2017).
4. T. Guo, W. Noble, D. P. Hanger, Roles of tau protein in health and disease. *Acta Neuropathol.* **133**, 665–704 (2017).
5. Y. Wang, E. Mandelkow, Tau in physiology and pathology. *Nat. Rev. Neurosci.* **17**, 5–21 (2016).
6. P. W. Baas, L. Qiang, Tau: It's not what you think. *Trends Cell Biol.* **29**, 452–461 (2019).
7. M. D. Mukrasch *et al*., Structural polymorphism of 441-residue tau at single residue resolution. *PLoS Biol.* **7**, e34 (2009).
8. E. M. Ingram, M. G. Spillantini, Tau gene mutations: Dissecting the pathogenesis of FTDP-17. *Trends Mol. Med.* **8**, 555–562 (2002).
9. K. H. Strang, T. E. Golde, B. I. Giasson, MAPT mutations, tauopathy, and mechanisms of neurodegeneration. *Lab. Invest.* **99**, 912–928 (2019).
10. S. Barghorn *et al*., Structure, microtubule interactions, and paired helical filament aggregation by tau mutants of frontotemporal dementias. *Biochemistry* **39**, 11714–11721 (2000).
11. M. von Bergen *et al*., Mutations of tau protein in frontotemporal dementia promote aggregation of paired helical filaments by enhancing local beta-structure. *J. Biol. Chem.* **276**, 48165–48174 (2001).
12. B. Combs, T. C. Gamblin, FTDP-17 tau mutations induce distinct effects on aggregation and microtubule interactions. *Biochemistry* **51**, 8597–8607 (2012).
13. S. Wegmann *et al*., Tau protein liquid-liquid phase separation can initiate tau aggregation. *EMBO J.* **37**, e98049 (2018).
14. J. C. Ferreon *et al*., Acetylation disfavors tau phase separation. *Int. J. Mol. Sci.* **19**, 1360 (2018).
15. S. Boyko, X. Qi, T. H. Chen, K. Surewicz, W. K. Surewicz, Liquid-liquid phase separation of tau protein: The crucial role of electrostatic interactions. *J. Biol. Chem.* **294**, 11054–11059 (2019).
16. N. M. Kanaan, C. Hamel, T. Grabinski, B. Combs, Liquid-liquid phase separation induces pathogenic tau conformations in vitro. *Nat. Commun.* **11**, 2809 (2020).
17. X. Zhang *et al*., RNA stores tau reversibly in complex coacervates. *PLoS Biol.* **15**, e2002183 (2017).
18. Y. Lin, Y. Fichou, Z. Zeng, N. Y. Hu, S. Han, Electrostatically driven complex coacervation and amyloid aggregation of tau are independent processes with overlapping conditions. *ACS Chem. Neurosci.* **11**, 615–627 (2020).
19. T. Ukmar-Godec *et al*., Lysine/RNA-interactions drive and regulate biomolecular condensation. *Nat. Commun.* **10**, 2909 (2019).
20. B. Wolozin, P. Ivanov, Stress granules and neurodegeneration. *Nat. Rev. Neurosci.* **20**, 649–666 (2019).
21. R. Tan *et al*., Microtubules gate tau condensation to spatially regulate microtubule functions. *Nat. Cell Biol.* **21**, 1078–1085 (2019).
22. X. Zhang, J. McCarty, J. N. Rauch, G. H. Fredrickson, M. Z. Wilson, J.-E. Shea, S. Han, K. S. Kosik, The proline-rich domain promotes tau liquid liquid phase separation in cells. *J. Cell Biol.* **219**, e202006054 (2020).
23. S.-G. Kang *et al*, Tau conformers in FTLD-MAPT undergo liquid-liquid phase separation and perturb the nuclear envelope .https://doi.org/10.1101/2020.07.04.187997 (5 July 2020).
24. T. Ukmar-Godec, S. Wegmann, M. Zweckstetter, Biomolecular condensation of the microtubule-associated protein tau. *Semin. Cell Dev. Biol.* **99**, 202–214 (2020).

25. A. Patel *et al*., A liquid-to-solid phase transition of the ALS protein FUS accelerated by disease mutation. *Cell* **162**, 1066–1077 (2015).
26. W. M. Babinchak *et al*., The role of liquid-liquid phase separation in aggregation of the TDP-43 low-complexity domain. *J. Biol. Chem.* **294**, 6306–6317 (2019).
27. S. Boeynaems *et al*., Protein phase separation: A new phase in cell biology. *Trends Cell Biol.* **28**, 420–435 (2018).
28. S. Elbaum-Garfinkle, Matter over mind: Liquid phase separation and neurodegeneration. *J. Biol. Chem.* **294**, 7160–7168 (2019).
29. V. H. Ryan, N. L. Fawzi, Physiological, pathological, and targetable membraneless organelles in neurons. *Trends Neurosci.* **42**, 693–708 (2019).
30. N. B. Nedelsky, J. P. Taylor, Bridging biophysics and neurology: Aberrant phase transitions in neurodegenerative disease. *Nat. Rev. Neurol.* **15**, 272–286 (2019).
31. W. M. Babinchak, W. K. Surewicz, Liquid-liquid phase separation and its mechanistic role in pathological protein aggregation. *J. Mol. Biol.* **432**, 1910–1925 (2020).
32. A. L. Darling, B. Y. Zaslavsky, V. N. Uversky, Intrinsic disorder-based emergence in cellular biology: Physiological and pathological liquid-liquid phase transitions in cells. *Polymers (Basel)* **11**, 990 (2019).
33. S. Alberti, A. Gladfelter, T. Mittag, Considerations and challenges in studying liquid-liquid phase separation and biomolecular condensates. *Cell* **176**, 419–434 (2019).
34. Y. Lin, D. S. Protter, M. K. Rosen, R. Parker, Formation and maturation of phase-separated liquid droplets by RNA-binding proteins. *Mol. Cell* **60**, 208–219 (2015).
35. R. A. Crowther, Straight and paired helical filaments in Alzheimer disease have a common structural unit. *Proc. Natl. Acad. Sci. U.S.A.* **88**, 2288–2292 (1991).
36. F. Ferrone, Analysis of protein aggregation kinetics. *Methods Enzymol.* **309**, 256–274 (1999).
37. E. T. Powers, D. L. Powers, The kinetics of nucleated polymerizations at high concentrations: Amyloid fibril formation near and above the "supercritical concentration". *Biophys. J.* **91**, 122–132 (2006).
38. W. Li, V. M. Lee, Characterization of two VQIXXK motifs for tau fibrillization in vitro. *Biochemistry* **45**, 15692–15701 (2006).
39. M. von Bergen *et al*., Assembly of tau protein into Alzheimer paired helical filaments depends on a local sequence motif ((306)VQIVYK(311)) forming beta structure. *Proc. Natl. Acad. Sci. U.S.A.* **97**, 5129–5134 (2000).
40. Q. Zhong, E. E. Congdon, H. N. Nagaraja, J. Kuret, Tau isoform composition influences rate and extent of filament formation. *J. Biol. Chem.* **287**, 20711–20719 (2012).
41. H. A. Weismiller *et al*., Structural disorder in four-repeat Tau fibrils reveals a new mechanism for barriers to cross-seeding of Tau isoforms. *J. Biol. Chem.* **293**, 17336–17348 (2018).
42. A. E. Conicella, G. H. Zerze, J. Mittal, N. L. Fawzi, ALS mutations disrupt phase separation mediated by α-helical structure in the TDP-43 low-complexity C-terminal domain. *Structure* **24**, 1537–1549 (2016).
43. A. Molliex *et al*., Phase separation by low complexity domains promotes stress granule assembly and drives pathological fibrillization. *Cell* **163**, 123–133 (2015).
44. V. H. Ryan *et al*., Mechanistic view of hnRNPA2 low-complexity domain structure, interactions, and phase separation altered by mutation and arginine methylation. *Mol. Cell* **69**, 465–479.e7 (2018).
45. I. R. Mackenzie *et al*., TIA1 mutations in amyotrophic lateral sclerosis and frontotemporal dementia promote phase separation and alter stress granule dynamics. *Neuron* **95**, 808–816.e9 (2017).
46. S. Flament, A. Delacourte, M. Verny, J. J. Hauw, F. Javoy-Agid, Abnormal Tau proteins in progressive supranuclear palsy. Similarities and differences with the neurofibrillary degeneration of the Alzheimer type. *Acta Neuropathol.* **81**, 591–596 (1991).
47. H. Ksiezak-Reding *et al*., Ultrastructure and biochemical composition of paired helical filaments in corticobasal degeneration. *Am. J. Pathol.* **145**, 1496–1508 (1994).
48. A. Delacourte *et al*., Specific pathological Tau protein variants characterize Pick's disease. *J. Neuropathol. Exp. Neurol.* **55**, 159–168 (1996).